Microvascular Research 58, 281–304 (1999)
Article ID mvre.1999.2177, available online at http://www.idealibrary.com on IDEAL®

A New View of Starling's Hypothesis at the Microstructural Level

Xiaping Hu and Sheldon Weinbaum

CUNY Graduate School and Department of Mechanical Engineering, The City College of The City University of New York, New York, New York 10031

Received October 26, 1998

In this paper we quantitatively investigate the hypothesis proposed by Michel (*Exp. Physiol.* 82, 1–30, 1997) and Weinbaum (*Ann. Biomed. Eng.* 26, 1–17, 1998) that the Starling forces are determined by the local difference in the hydrostatic and colloid osmotic pressure across the endothelial surface glycocalyx, which we propose is the primary molecular sieve for plasma proteins, rather than the global difference in the hydrostatic and oncotic pressure across the capillary wall between the plasma and tissue, as has been universally assumed until now. A spatially heterogeneous microstructural model is developed to explain at the cellular level why there is oncotic absorption at low capillary pressures in the short-lived transient experiments of Michel and Phillips (*J. Physiol.* 388, 421–435, 1987) on frog mesentery capillary, but a small positive filtration once a steady state is achieved. The new model also predicts that the local protein concentration behind the surface glycocalyx can differ greatly from the tissue protein concentration, since the convective flux of proteins through the orifice-like pores in the junction strand will greatly impede the back diffusion of the proteins into the lumen side of the cleft when the local Peclet number at the orifice is >1. The net result is that the filtration in the capillaries is far less than heretofore realized and there may be no need for venous reabsorption.

Key Words: capillary osmotic pressure; surface glycocalyx; fiber matrix; venous reabsorption; capillary filtration.

INTRODUCTION

Michel (1997) and Weinbaum (1998) proposed a new cellular level model for the effective osmotic barrier that acts across capillary endothelium and the role of small pores in the interendothelial cleft in determining the Starling forces and lymph flow in most tissues whose primary function is not reabsorption. In this spatially heterogeneous microstructural model the endothelial surface glycocalyx serves as the primary molecular filter for plasma proteins and, thus, the principal barrier that determines the effective oncotic force for water flow across capillary endothelium. According to this hypothesis the local Starling forces that determine the water flux across capillary endothelium are due to the local difference in hydraustatic and oncotic pressure across the surface matrix layer rather than the global difference in P and π between plasma and tissue. These ideas were first quantitatively explored in the 1997 Whitaker Distinguished Lecture, (Weinbaum, 1998), where preliminary results for a detailed cellular level microstructural model are presented. In the present paper this mathematical model is more fully developed. Detailed calculations are presented for Michel and Phillips' (1987) experiment on single perfused frog mesentery capillaries and for the case where there is a parallel nonconvective large pore transcellular pathway for albumin. This pathway in-

0026-2862/99 $30.00

creases the tissue concentration to values typical of those estimated by Levick (1991) for mammalian capillaries. For the latter case we explore the possibility that the presence of the junction strand with its small pore openings might shield the region between the backside of the surface matrix and the junction strand from the concentration in the tissue space. Such shielding would uncouple the large and small pore pathway as suggested by Michel (1997).

Starling's hypothesis is universally described by an equation of the form

$$J_v / A = L_p[(P_c - P_i) - \sigma(\pi_c - \pi_i)], \qquad (1)$$

where J_v / A is the fluid filtration rate across the capillary wall per unit area, L_p is hydraulic permeability of the capillary wall, σ is the osmotic reflection coefficient, and P_c, π_c and P_i, π_i are global values for the hydrostatic and colloidal osmotic pressures in the plasma and tissue, respectively.

According to the microstructural measurements of frog mesentery capillaries by Adamson and Michel (1993), the typical dimensions of the small pores in the junction strand in the transendothelial cleft are 150∗20 nm. Compared with the effective diameter of albumin, 7 nm, these pores are too large to be the molecular filter. We thus explore the possibility that the primary sieving layer for albumin, at least in frog mesentery, is the surface glycocalyx, as proposed by Michel (1997) and Weinbaum (1998).

In our new model, Eq. (1) will be applied locally across the surface matrix layer, and π_i will be replaced by the local protein oncotic pressure on the tissue side of the matrix layer. Similarly, the pressure P_i that appears in Eq. (1) will be replaced by the local pressure behind the surface glycocalyx, where the effective oncotic pressure is felt. This change will have a substantial effect on the predicted magnitude of the Starling forces and lead to major changes in the classical Landis–Starling diagram. The model has some similarity to that proposed by Taylor and Townsley (1987) in that P_i and π_i are spatially varying. The fundamental difference is that the spatial heterogeneity is not on the length scale of the capillary length, as proposed by Taylor and Townsley (1987), but on a microstructural length scale associated with the junction strand structure.

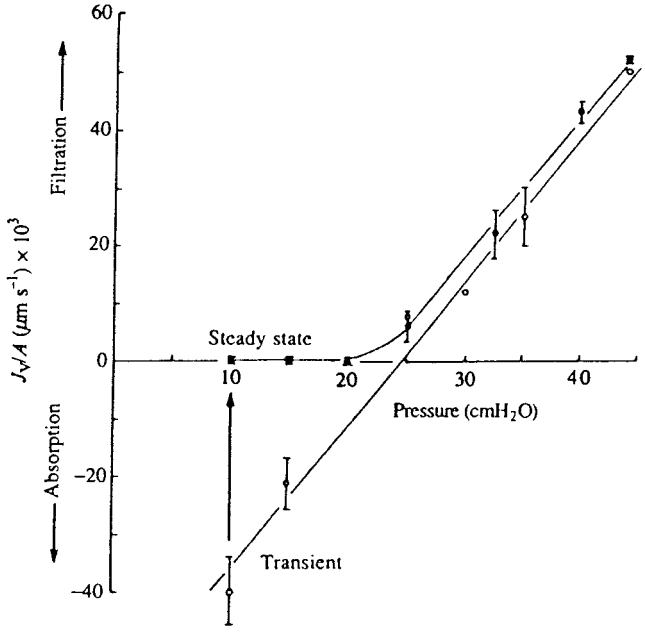

FIG. 1. Water flux J_v / A in a single perfused frog mesentery capillary as a function of capillary pressure. For the transient state, measurements are performed in the first 15–30 s after the perfusion pressure is fixed, and for the steady state, measurements are performed 2 to 5 min after the perfusion pressure is fixed. Reprinted, with permission, from Michel and Phillips, 1987.

Several investigators (Michel, 1984; Taylor and Townsley, 1987; Levick, 1991) have recognized that interstitial hydraulic pressure and interstitial oncotic pressure are dynamic variables which depend on microvascular fluid flux as well as being a determinant of it. In 1987, Michel and Phillips performed a pioneering experiment on isolated frog mesentery microvessels. The variation of J_v / A with P_c was measured while maintaining a constant oncotic pressure in the perfusate. The essential results of this experiment are shown in Fig. 1. Two fundamentally different behaviors were observed. One was a short-lived transient behavior when measurements were made within 15 to 30 s after the pressure was quickly reduced from its maximum value of 43 cm H_2O to some lower value and the tissue washed in protein-free Ringer. The second was a steady-state behavior that was obtained 2 to 5 min after the pressure P_c was changed and maintained constant until a new equilibrium was achieved. In the transient case the results were consistent with a classical Landis–Starling diagram in which there is arterial

filtration at high capillary pressure and venous reabsorption at low capillary pressure. One observes a critical pressure for no flow, 24 cm H_2O, and J_v/A varies linearly with P_c about this value. In contrast, in the steady-state experiments the net fluid flow followed the transient behavior when P_c exceeded the perfusate oncotic pressure, whereas there was no absorption but a small net positive filtration for all values of P_c below about 20 cm H_2O. This nonlinear relationship in the steady state is also consistent with the experiments of Guyton and Lindsey (1959) and Perl *et al.* (1975) on the accumulation of fluid in dog lungs when the left atrial pressure is varied. The former observed that at atrial pressures above 25 mm Hg fluid leaves the capillaries and enters the lung tissue and lung weight varies linearly with the atrial pressure and that at pressures below 25 mm Hg the lung weight remains almost constant.

Michel and Phillips, in their 1987 paper, developed a simple, but very insightful, one-dimensional model to explain these surprising observations. For the transient case they assumed the tissue osmotic pressure, π_i, was effectively zero, since if the hydraulic pressure is quickly dropped, there is insufficient time for the interstitial oncotic pressure to adjust and absorption will occur, whereas if the reduced hydrostatic pressure is maintained, the absorption across the vessel should gradually decrease as solute enters the tissue space until a new steady-state equilibrium is achieved. Only if there is a higher filtration flow into the interstitium, as in the kidney or intestine, can absorption be sustained (Michel, 1984). For the steady case Michel calculated π_i by assuming that the convection through the capillary wall would eventually establish a condition in the tissue where the protein concentration C_i would eventually achieve an equilibrium value $C_i = J_s/J_v$, determined by the total water and solute fluxes into the tissue space. Here, J_s is the total protein flux across the capillary endothelium including both diffusion and convection, and J_v is the total fluid flux across the capillary. This relation for C_i would apply if the tissue outside the vessel behaved as a well-stirred reservoir in which all the water and proteins passing through the capillary endothelium were thoroughly mixed and there was a uniform protein concentration in the tissue.

An important issue raised in Taylor and Townsley (1987) and Levick (1994) is the spatial heterogeneity of the fluid and protein fluxes in the tissue space at the cleft exit. Michel and Phillips in their one-dimensional model (1987) assumed that the water and solute flux are spatially uniform. However, it is clear from the junction ultrastructure of frog mesentery capillary (Adamson and Michel, 1993) that there is spatial heterogeneity in the water flux along the length of the cleft. Levick (1994) had previously developed a model to examine the effect of local water fluxes through the discrete fenestra of synovial capillaries on near-pore oncotic and hydraulic gradients. He showed that the local flow across fenestrae will dilute the solute immediately outside the fenestrae and thus reduce the local Starling forces in the interstitium. The magnitude of this reduction is, however, small compared to that which can be achieved for continuous capillaries where there is a protective barrier with small pores that prevent back diffusion. A similar analysis to Levick (1994) is developed by Fu *et al.* (1997) for continuous capillaries. Concentration profiles for the nonuniformity in cleft exit concentration due to convection are predicted, but these are uncoupled from the local oncotic forces that determine the water flow across the surface matrix. In this paper, we will provide a detailed picture as to how these water and solute fluxes relate to cellular level structure, namely the sieving matrix at the endothelial surface, the interendothelial cleft with its junction strand, and the mixing region at the cleft exit. We shall also examine how the uniformity in protein concentration assumed in Michel's expression for C_i is achieved and what would happen if there were other parallel nonselective large pore transcellular pathways for protein flux due to active vesicular transport, connected vesicle channels, or transient gaps in the endothelium due to inflammatory agents.

MODEL DESCRIPTION

From an ultrastructural viewpoint the idealized model that has been proposed to explore the new hypothesis for the Starling forces is similar to earlier models developed (Fu *et al.*, 1994, 1997; Weinbaum *et*

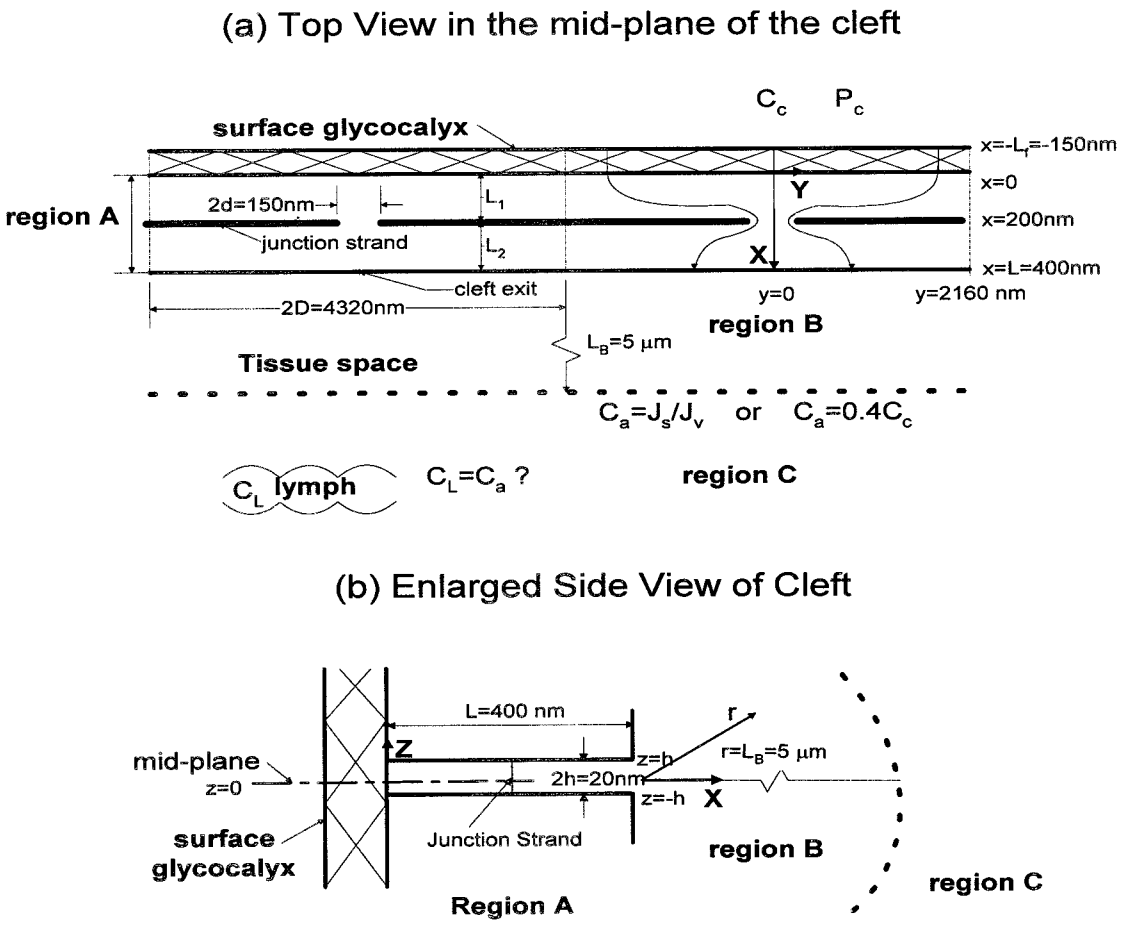

FIG. 2. (a) Schematic of idealized mathematical model showing surface matrix layer, cleft region A with junction strands, and tissue regions B and C describing mixing at cleft exit. Dimensions shown are typical for frog mesentery capillary. (b) Side view of the cleft showing cleft height and the location of the cleft midplane.

al., 1992) to predict the capillary filtration and diffusive permeability coefficients, L_p and P, in frog mesentery capillary in terms of the structure of the interendothelial cleft and the endothelial surface glycocalyx. A schematic of this model is shown in Fig. 2. This ultrastructural model differs from our earlier studies only in that it neglects the narrow continuous 1.5-nm slit in the junction strand proposed by Fu *et al.* (1994). This narrow slit could also serve as an osmotic barrier. However, it would allow only a small additional water flux due to its large hydraulic resistance. Furthermore, Fu *et al.* (1998) have shown that a small tracer, Na fluorescein (0.8 nm), does not appear to cross this barrier indicating that if the slit is patent its gap height is significantly less than 1.5 nm.

The model in Fig. 2 contains four regions. The first region is a surface glycocalyx of thickness L_f which covers the entire endothelial surface including the entrance region to the interendothelial cleft. Using cationized ferritin as a tracer to delineate the outer regions of this surface matrix, Adamson and Clough (1992) have estimated from electromicrographs that this surface layer is of roughly 0.1-μm thickness in frog mesentery capillary. Furthermore, if this layer is to serve as the molecular sieve for proteins the size of albumin or larger, then the spacing of the fibers in this matrix is approximately 7 nm. An even thicker surface layer of 0.4 to 0.5 μm is observed *in vivo* in hamster cremaster capillaries (Vink and Duling, 1996). However, the theoretical model of Fu *et al.* (1994) predicts

that a sieving matrix layer of this thickness would offer too much hydraulic resistance for frog mesentery capillary and that a more accurate estimate for this tissue is 0.1 μm. The second region is the cleft proper, region A which extends from $x = 0$ to $x = L$, the depth of the cleft. Serial section reconstructions of the junction strand in frog mesentery (Adamson and Michel, 1993) reveal a junction strand with discontinuous breaks or pores that are on average 150 nm long with a spacing that varies between 2 and 5 μm. The depth of the cleft is 0.4 μm and the gap height of the breaks, 20 nm, is the same as the nearly uniform wide part of the cleft.

In the model the pericapillary space is broken into two regions, a semicircular region B of 5-μm radius which surrounds the cleft exit, and a far field, region C. The radius of region B, L_B, is determined by the average spacing of the clefts, 10 μm, along the cross-sectional perimeter of the capillary. Region B describes the mixing of the wakes from the individual junction strand discontinuities in the tissue space immediately surrounding the cleft exit. In the event that there is an additional nonselective parallel pathway for plasma proteins, the concentration at the edge of region B can be elevated and its value specified. To explore what would happen if there were a large pore parallel pathway, we shall assume a typical value for C_a that has been measured in many mammalian tissues, 0.4 C_c (Levick, 1991). In region C, the exit jets from the individual junction orifices and adjacent clefts merge with each other and form a uniform flux along the length of the cleft exit in the tissue space beyond region B. Therefore, region C can be approximated by a one-dimensional convection–diffusion model averaged across the height (thickness) of the tissue layer.

METHODS

1. *Pressure and Velocity Field*

(1) Fiber matrix layer. The fiber matrix layer lies in front of the cleft and covers the entire endothelial surface. This continuous fiber layer is assumed to have a uniform thickness L_f. For pure filtration, Darcy's law can be applied locally across the fiber layer along the length of the cleft in the y direction.

$$\bar{V}(y) = \frac{K_p}{\mu}\frac{P_c - P(0, y)}{L_f}. \quad (2)$$

Here K_p is the Darcy permeability, μ is the fluid viscosity, and $\bar{V}(y)$ is the local average velocity at location y. P_c and $P(0, y)$ are pressures in the lumen and at the entrance to the cleft behind the surface glycocalyx, respectively. This simple one-dimensional approximation can be applied across the surface matrix because pressure gradients, and hence velocities, in the x direction are nearly two orders of magnitude greater than in the y direction.

If plasma proteins are present the local velocity across the fiber matrix layer is the resultant of two opposing forces, a hydraulic filtration pressure and an oncotic force. If the local oncotic force across the surface layer is considered, Eq. (2) can be written as

$$\bar{V}(y) = \frac{K_p}{\mu L_f}[P_c - P(0, y) - \sigma_f(\pi_c - \pi(0, y))], \quad (3)$$

where σ_f is the reflection coefficient in the fiber matrix. $\pi(0, y)$ and π_c are osmotic pressures just behind the fiber matrix at $x = 0$ and in the lumen, respectively. The relation between albumin osmotic pressure π (cm H_2O) and free-fluid concentration C (g/liter) is given as

$$\pi = 0.345C + 2.657 \times 10^{-3} C^2 + 2.26 \times 10^{-5} C^3. \quad (4)$$

This polynomial describes the nonlinear relationship between π and C at higher albumin concentrations determined by a curve fit of experimental data given by McDonald and Levick (1993).

Note that both $P(0, y)$ and $\pi(0, y)$ vary along the length of the cleft entrance in Eq. (3). Equation (3) differs fundamentally from Eq. (1) in that it is applied locally across just the surface sieving layer, rather than in a global sense across the entire endothelial layer.

(2) Region A; cleft. Region A can be split into two subregions. Region 1 with depth L_1, $0 \leq x \leq 200$ nm, lies upstream of the junction strand behind the fiber matrix layer and region 2 with depth L_2 lies down-

stream of the junction strand, $200 \le x \le 400$ nm. The thickness of the junction strand can be neglected compared to L_1 and L_2 and treated as a zero-thickness barrier; see Fig. 2.

Since the height of the cleft $2h$ is small compared to both the average distance between the pores $2D$ and the depths L_1 and L_2 of the cleft, the water flow in the wide part of the cleft can be approximated by a Hele–Shaw flow as first proposed by Tsay and Weinbaum (1989). Thus the velocity in the cleft can be expressed as

$$\begin{aligned} &\mathbf{V}(x, y, z) = \mathbf{V}_0(x, y)\left(1 - \frac{z^2}{h^2}\right) \quad \text{and} \\ &\mathbf{V}(x, y, z) = u(x, y, z)\mathbf{i} + v(x, y, z)\mathbf{j} + 0\mathbf{k}, \end{aligned} \tag{5a}$$

which satisfies the nonslip condition $u = v = 0$ at $z = \pm h$; see Fig. 2b. $\mathbf{V}_0(x, y)$, the velocity in the center plane $z = 0$, is given by

$$\begin{aligned} &\mathbf{V}_0(x, y) = -\frac{h^2}{2\mu}\nabla P \quad \text{and} \\ &\mathbf{V}_0(x, y) = u_0(x, y)\mathbf{i} + v_0(x, y)\mathbf{j}. \end{aligned} \tag{5b}$$

For Hele–Shaw flow, the pressure in the cleft satisfies

$$\frac{\partial^2 P}{\partial x^2} + \frac{\partial^2 P}{\partial y^2} = 0. \tag{6}$$

Note that a two-dimensional pressure field is required to describe the flow in the cleft although L_1 and L_2 are not much greater than the thickness L_f of the matrix layer. This is required because pressure gradients in the x and y directions become comparable at the junction orifice due to the convergence of the fluid streamlines.

At $x = 0$, the pressure and u component of velocity at the rear of the surface matrix layer must equal the pressure and average value of u at the cleft entrance. The flow behind the matrix has a slip plane for the v component of the velocity. This is quite realistic since this slip occurs over a distance which is about half the channel height (Fu *et al.*, 1994). This thin fiber interaction layer is small compared to the half depth of the cleft. Integrating Eq. (5a) over the height of the cleft, one finds that the average velocity $\bar{\mathbf{V}}(x, y)$ is given by $\bar{\mathbf{V}}(x, y) = \frac{2}{3}\mathbf{V}_0(x, y)$.

Combining Eqs. (3), (5a), and (5b), one obtains the first matching condition at $x = 0$:

$$P_c - P(0, y) - \sigma_f(\pi_c - \pi(0, y)) = -\frac{h^2 L_f}{3K_p}\frac{\partial P^{(1)}}{\partial x}\bigg|_{x=0^+}. \tag{7a}$$

One notes that $P(0, y)$, $\pi(0, y)$ and $\partial P^{(1)}/\partial x|_{x=0^+}$ are all unknown and Eq. (7a) is a nonlinear coupling condition. The other boundary and matching conditions for Eq. (6) are

$$x = L_1 \qquad d < |y| \le D \qquad \frac{\partial P^{(i)}}{\partial x} = 0 \qquad i = 1, 2 \tag{7b}$$

$$x = L_1 \qquad |y| \le d \qquad P^{(1)} = P^{(2)} \qquad \frac{\partial P^{(1)}}{\partial x} = \frac{\partial P^{(2)}}{\partial x} \tag{7c}$$

$$x = L \qquad |y| \le D \qquad P^{(2)} = P_i \tag{7d}$$

$$0 \le x \le L \qquad y = 0, D \qquad \frac{\partial P^{(i)}}{\partial y} = 0 \qquad i = 1, 2. \tag{7e}$$

Boundary conditions (7b) and (7c) require that the junctional strand be impermeable except at the junctional break and the pressure and velocity across the junctional breaks be continuous. Boundary condition (7d) requires that the pressure be continuous at the tissue front. Boundary conditions (7e) are the periodicity and symmetry conditions.

Interstitial hydraulic resistance is of minor importance in the present application because of the high permeability of interstitial matrix compared to the capillary wall. Therefore, the pressure drop in regions B and C will be neglected and a uniform pressure P_i is assumed which is -2 cm H_2O (Guyton, 1963).

2. *Concentration Field*

(1) Fiber matrix layer. One-dimensional convection–diffusion is assumed locally across the surface matrix layer in front of the cleft entrance. The results of our model show that concentration gradients in the x direction in the matrix layer are more than two orders of magnitude greater than in the y direction. The governing equation for solute conservation is, therefore,

$$D_f \frac{\partial^2 C(x, y)}{\partial x^2} = \bar{u}_s(y) \frac{\partial C(x, y)}{\partial x}, \quad (8)$$

where $\bar{u}_s(y)$, the solute average velocity in the cleft, is related to $u_0(0, y)$, the water velocity in the center plane by $\bar{u}_s(y) = \frac{2}{3}\chi_f u_0(0, y)$. Here χ_f and D_f are the retardation and effective solute diffusion coefficients in the matrix layer, respectively.

The boundary and matching conditions for Eq. (8) are

$$x = -L_f \quad C = C_c, \quad (9a)$$

$$x = 0 \qquad C = C(0, y), \quad (9b)$$

$$-D_f \frac{\partial C}{\partial x}\bigg|_{x=0^-} + \frac{2}{3}\chi_f u_0(0, y) C(0, y) = -D_c \frac{\partial C}{\partial x}\bigg|_{x=0^+} + \frac{2}{3}\chi_c u_0(0, y) C(0, y), \quad (9c)$$

where χ_c and D_c are their values in the wide part of the cleft. Boundary conditions (9b) and (9c) require that the protein concentration and solute flux be continuous at the cleft entrance, $x = 0$.

Solving Eq. (8) subject to boundary conditions (9a) and (9b), we find

$$C = \frac{C_c - C(0, y)}{1 - e^{-\mathrm{Pe}_f}} (1 - e^{\mathrm{Pe}_f(x/L_f)}) + C(0, y), \quad (10)$$

where

$$\mathrm{Pe}_f = \frac{2}{3} \frac{\chi_f u_0(0, y) L_f}{D_f} \quad (11)$$

is the local Peclet number in the surface matrix layer.

Substituting Eq. (10) into Eq. (9c), one obtains a second nonlinear coupling condition between velocity and protein concentration at the rear of the surface glycocalyx:

$$D_f \left(\frac{C_c - C(0, y)}{1 - e^{-\mathrm{Pe}_f}} \right) \frac{\mathrm{Pe}_f}{L_f} + \frac{2}{3}\chi_f u_0(0, y) C(0, y) = -D_c \frac{\partial C}{\partial x}\bigg|_{x=0^+} + \frac{2}{3}\chi_c u_0(0, y) C(0, y). \quad (12)$$

Note that $C(0, y)$, $u_0(0, y)$, and $P(0, y)$ are all unknown and nonlinearly coupled through Eqs. (7a) and (12). They cannot be solved for separately, but must be determined by the solution of the overall boundary value problem for u, P, and C.

(2) Region A; cleft. The governing equation for solute concentration in the cleft can be approximated by a steady two-dimensional convection–diffusion equation averaged across the cleft height:

$$D_c \left(\frac{\partial^2 C(x, y)}{\partial x^2} + \frac{\partial^2 C(x, y)}{\partial y^2} \right) = \frac{2}{3}\chi_c \left(u_0(x, y) \frac{\partial C(x, y)}{\partial x} + v_0(x, y) \frac{\partial C(x, y)}{\partial y} \right). \quad (13)$$

A two-dimensional concentration field must be used to describe the cleft since x and y gradients and velocity components are of comparable magnitude in the vicinity of the junction strand orifice.

In addition to Eqs. (7a) and (12) the remaining boundary and matching conditions for solute transport for Eq. (13) are

$$x = L_1 \quad |y| \le d \quad C^{(1)} = C^{(2)} \quad \frac{\partial C^{(1)}}{\partial x} = \frac{\partial C^{(2)}}{\partial x}, \quad (14a)$$

$$x = L_1^- \quad d < |y| \le D \quad -D_c \frac{\partial C^{(1)}}{\partial x} + \frac{2}{3}\chi_c u_0 C^{(1)} = 0 \quad (14b)$$

$$x = L_1^+ \quad d < |y| \le D \quad -D_c \frac{\partial C^{(2)}}{\partial x} + \frac{2}{3}\chi_c u_0 C^{(2)} = 0, \quad (14c)$$

$$x = L \quad |y| \le D \quad \left(-D_c \frac{\partial C^{(2)}}{\partial x} + \frac{2}{3}\chi_c u_0 C^{(2)} \right)\bigg|_{x=L} * 2h = q(y), \quad (14d)$$

$$0 \le x \le L \quad y = 0, D \quad \frac{\partial C^{(i)}}{\partial y} = 0 \quad i = 1, 2. \quad (14e)$$

Boundary conditions (14a)–(14c) require that the junctional strand be impermeable except for the pore region $|y| \le d$. Matching condition (14d) is the equation for the local solute flux $q(y)$ entering the tissue at the cleft exit. Boundary conditions (14e) are the periodicity and symmetry conditions.

(3) Region B; cleft exit near field. The average distance between neighboring clefts in the vessel wall is typically 10 μm. The gap height of the wide part of the cleft is merely 20 nm, which is much smaller than the

radius of region B, 5 μm. Thus, the solute flux at the cleft exit can be treated as a line source of variable strength along the length of the cleft exit in the y direction. Since gradients in the y direction near the cleft exit are smaller than radial gradients, the governing equation for this region is

$$D_t\left(\frac{\partial^2 C(r, y)}{\partial r^2} + \frac{1}{r}\frac{\partial C(r, y)}{\partial r}\right) = \chi_t v_r \frac{\partial C(r, y)}{\partial r}, \quad (15)$$

where r is measured from $x = L$ and $z = 0$ in Fig. 2b. Here D_t and χ_t are the solute diffusion and the protein retardation coefficients in the tissue and v_r is the radial velocity in region B. As the solute spreads from the cleft exit y gradients do become comparable to r gradients, but here the results show that both gradients are greatly reduced and Eq. (15) is still a reasonable if not accurate approximation.

The boundary and matching conditions for Eq. (15) are Eq. (14d) and

$$C^{(2)}|_{x=L} = C|_{r=h} \text{ at } r = h, \quad (16a)$$

$$\left(-D_t\frac{\partial C}{\partial r} + \chi_t v_B C\right)\Big|_{r=h} * \pi h = q(y) \quad \text{at } r = h, \quad (16b)$$

$$C(L_B) = C_a \qquad \text{at } r = L_B. \quad (16c)$$

Here $r = h$ and L_B are the inner and outer radii of the intermediate region B. L_B is the average half spacing between adjacent clefts, and $q(y)$, the local solute flux at the cleft exit, is obtained from Eq. (14d). C_a is the solute concentration at the interface between regions B and C.

From simple continuity arguments, the radial velocity in the intermediate region B, v_r, decays as $1/r$, if the lateral spread of the cleft exit jet in the y direction is neglected. This is a reasonable approximation for a line source that is slowly varying along its length. Thus,

$$v_r(r, y) = \frac{h}{r} v_B(y), \quad (17a)$$

where

$$v_B(y) = \frac{4}{3\pi} u_0(x, y)|_{x=L} \quad (17b)$$

is the locally varying average velocity at $r = h$, the cleft exit.

In the absence of convection, $v_r = v_B = 0$, the solution of Eq. (15) for the concentration in the tissue in region B is

$$C(r, y) = \frac{q(y)}{\pi D_t}\ln(L_B/r) + C_a. \quad (18)$$

If $v_r \neq 0$, the solution to Eq. (15) which satisfies Eqs. (16b), (16c), and (17) is

$$C(r, y) = C_a\left(\frac{r}{L_B}\right)^{Pe_t} + \frac{q(y)}{\pi B \chi_t v_B}\left[1 - \left(\frac{r}{L_B}\right)^{Pe_t}\right], \quad (19a)$$

where

$$Pe_t = \frac{\chi_t v_B h}{D_t}. \quad (19b)$$

If there is a parallel nonselective pathway through the vessel wall, such as vesicular transport, the protein concentration in the tissue will be elevated. In this case the concentration at $r = L_B$ will be prescribed and we shall use the estimate $C(L_B) \cong 0.4C_c$ suggested by the data obtained by Levick (1991). For the case where $C_i = J_s/J_v$, as proposed by Michel and Phillips (1987), C_a is unknown and provides a matching condition with region C, which is described next.

(4) Region C; tissue space far field. In region B the exit jets from the individual junction orifices and adjacent clefts merge with each other and form a uniform flux along the length of the cleft exit. Therefore, region C for frog mesentery can be approximated by a one-dimensional convection–diffusion equation averaged across the height of the tissue layer H,

$$D_t\frac{d^2C(x)}{dx^2} = \chi_t v_c \frac{dC(x)}{dx}. \quad (20)$$

The boundary conditions for Eq. (20) are

$$-D_t\frac{dC(x)}{dx} + \chi_t v_c C(x) = q_c \quad \text{at} \quad x = 0, \quad (21a)$$

$$C = C_i \quad \text{at} \quad x = L_c, \quad (21b)$$

where q_c is average solute flux per unit tissue area normal to the flow direction. q_c is given by

$$q_c = \frac{N_c}{2H}\frac{J_s}{D}, \tag{22}$$

where N_c is the number of clefts on the half surface of the vessel and H is the height of the tissue layer. J_s, the average flux per unit cleft length, is given by Eq. (A3) in the Appendix. v_c in Eq. (21) is the average velocity in region C which can be expressed as

$$v_c = \frac{N_c}{2H}\frac{J_v}{D}, \tag{23}$$

where J_v, the average water flux per unit cleft length, is given by Eq. (A4) in the Appendix.

The solution to Eq. (20) subjected to the boundary conditions (21a) and (21b) is

$$C = \left(C_i - \frac{q_c}{\chi_t v_c}\right) e^{(\chi_t v_c / D_t)(x - L_c)} + \frac{q_c}{\chi_t v_c}. \tag{24}$$

Substituting $x = 0$ into Eq. (24) and evaluating the solute concentration at the edge of region B, one obtains

$$C_a = \left(C_i - \frac{q_c}{\chi_t v_c}\right) e^{-(\chi_t v_c / D_t) L_c} + \frac{q_c}{\chi_t v_c}. \tag{25}$$

For Michel and Phillips' (1987) experiment Eq. (25) relates the concentration C_a to the concentration $C_i = J_s / J_v$, which is given by Eq. (A5) in the Appendix.

(5) Method of solution. The original boundary value problem, which was formidable due to the nonlinearity of the equations and matching conditions and the different length scales of the four different regions in Fig. 2, has been greatly simplified by the analytic solutions for the surface matrix layer and regions B and C in the tissue. The overall boundary value problem has been reduced to that of obtaining a numerical solution, albeit for a system of nonlinear equations and boundary conditions, for a single region, the cleft itself, region A. Regions B and C could have been treated numerically using a two-dimensional computer code but this would have greatly expanded computational costs with no new insight into the essential physics.

The simplified boundary value problem for region A just described has been solved using a time-dependent relaxation technique. Instead of solving Eqs. (6) and (13), we solve an initial value problem for their time-dependent counterparts,

$$\frac{\partial P}{\partial t} = \frac{\partial^2 P}{\partial x^2} + \frac{\partial^2 P}{\partial y^2} \tag{26}$$

and

$$\frac{\partial C}{\partial t} = D_c\left(\frac{\partial^2 C}{\partial x^2} + \frac{\partial^2 C}{\partial y^2}\right) - \tfrac{2}{3}\chi_c\left(u_0\frac{\partial C}{\partial x} + v_0\frac{\partial C}{\partial y}\right). \tag{27}$$

When t approaches infinity, P and C relax to their steady-state values, i.e., $\partial P/\partial t = 0$ and $\partial C/\partial t = 0$, which is the solution of the original problem. Finite-difference approximations are employed for the derivatives in Eqs. (26) and (27) and the corresponding boundary conditions, Eqs. (7), (12), and (14). Arbitrary initial conditions can be used at each point. For convenience, we have assumed uniform pressure and concentration as initial conditions in the cleft. During each iteration, pressure and concentration at each mesh point are calculated from difference equations derived from Eqs. (26) and (27), except for boundary mesh points which are required to satisfy the matching conditions and boundary conditions given by Eqs. (7), (12), and (14). Because the pressure and concentration fields are coupled, these two fields are calculated simultaneously. The numerical solution is advanced in time until every mesh point converges and satisfies a convergence condition that the relative error between the nth and $(n + 1)$th iteration values for P and C at each point, $|(P^{(n+1)} - P^{(n)})/P^{(n)}|$ and $|(C^{(n+1)} - C^{(n)})/C^{(n)}|$, differ by less than 10^{-6}.

PARAMETER VALUES

1. Parameter Values for Anatomical Structure

The thickness of fiber matrix layer $L_f = 150$ nm and the average spacing of these breaks $2D = 4320$ nm has been chosen to satisfy for measured value of $L_p = 2.46{*}10^{-7}$ cm/s/cm H_2O (Michel and Phillips, 1987). The other values for describing the cleft geometry in Fig. 2 are the same as those of Fu *et al.* (1994), which

are based on the measurements for frog mesentery vessels. The cleft depth $L = 400$ nm and height of the wide part of the cleft $2h = 20$ nm. Junction breaks $2d*2h = 150$ nm$*$20 nm are centered at $y = 0$. The radius of region B $L_B = 5$ μm. The length of region C, 100 μm, is a typical half spacing for frog mesentery capillaries.

2. Parameter Values for Transport

The osmotic reflection coefficient for albumin in the fiber matrix $\sigma_f = 0.9$ (Michel and Phillips, 1987). Since the molecular radius of Ficoll 70 is a little larger than that of albumin, $\sigma_f = 0.94$ is assumed for Ficoll 70. A reasonable value for the reflection coefficient in the cleft for either molecule is $\sigma_c = 0.1$. This estimate is based on calculations for the hydrodynamic interaction of a sphere with the plasmalemma boundaries. There are few measured values for the interstitial reflection coefficient. In this paper, we have used the simplifying assumption that $\sigma_t = 0$ and $\chi_t = 1$ in the absence of better data.

An approximate theory for determining the diffusion coefficient D_f in a fiber matrix which takes account of both the hydraulic resistance and the steric hindrance of the fibers is given by Weinbaum *et al.* (1992). However, there is no adequate theory to predict the diffusion coefficient, when proteins are of comparable or larger size than the fiber spacing or if the fibers are not rigid. In this paper, we have been able to circumvent this difficulty by requiring the model to provide an optimum fit of the steady-state filtration profile obtained in Michel's experiment shown in Fig. 1. This comparison is shown in Fig. 10 of this paper and will be discussed later in greater detail. The model predicts a dense matrix whose value for D_f for albumin is three to four orders of magnitude smaller than its value in solution. This value of D_f refers only to the matrix at the entrance to the cleft pathway and should not be confused with the total measured permeability. The latter also includes active transport of albumin, vesicle channels, and transient endothelial gaps. The diffusion coefficient D_c in the cleft is a restricted diffusivity given by Ganatos (1981) for a sphere diffusing in a channel without a matrix. The wide part of the cleft can be thought of as an adherens junction that contains cross bridging proteins. This should not greatly decrease D_c since these proteins either appear in localized regions or are widely dispersed. We have estimated the diffusion coefficient in the tissue D_t as $0.13D_\infty$, which is based on the measured value $D_t/D_\infty = 0.14$ for dextran fluorescein isothiocyanate 19,100 (Stokes radius = 3.12 nm) (Fox and Wayland, 1979).

RESULTS

To facilitate the discussion in the next section the results are presented under three headings: (1) mathematical modeling of Michel and Phillips' experiments, (2) analysis of parallel pathway, and (3) effect of D_f on filtration–pressure curve.

1. Mathematical Modeling of Michel and Phillips' Experiments

Key results corresponding to Michel and Phillips' (1987) steady-state and transient experiments in Fig. 1 are shown in Figs. 3–6 where detailed profiles are presented for the pressure, velocity, and protein concentration profiles for three representative conditions: (A) high capillary pressure, (B) low capillary pressure steady state, and (C) low capillary pressure transient state. The results in Fig. 3 are for a high filtration state corresponding to a high capillary pressure of $P_c = 43$ cm H_2O. In this high filtration state, there is a little difference between the steady state and transient results in Fig. 1. The results in Figs. 4 and 5 show representative solutions for the steady-state and transient profiles, respectively, corresponding to a low capillary pressure of $P_c = 15$ cm H_2O, typical of venous capillaries, where one would normally anticipate venous reabsorption.

Pressure and concentration profiles are plotted at $x = -L_f$, in front of the surface matrix layer where we assume that the pressure and concentration are constant; $x = 0$, just behind the fiber matrix layer at the cleft entrance; $x = 200^-$ nm and $x = 200^+$ nm, just upstream and downstream of the junction strand, and $x = 400$ nm, the cleft exit where the tissue pressure is

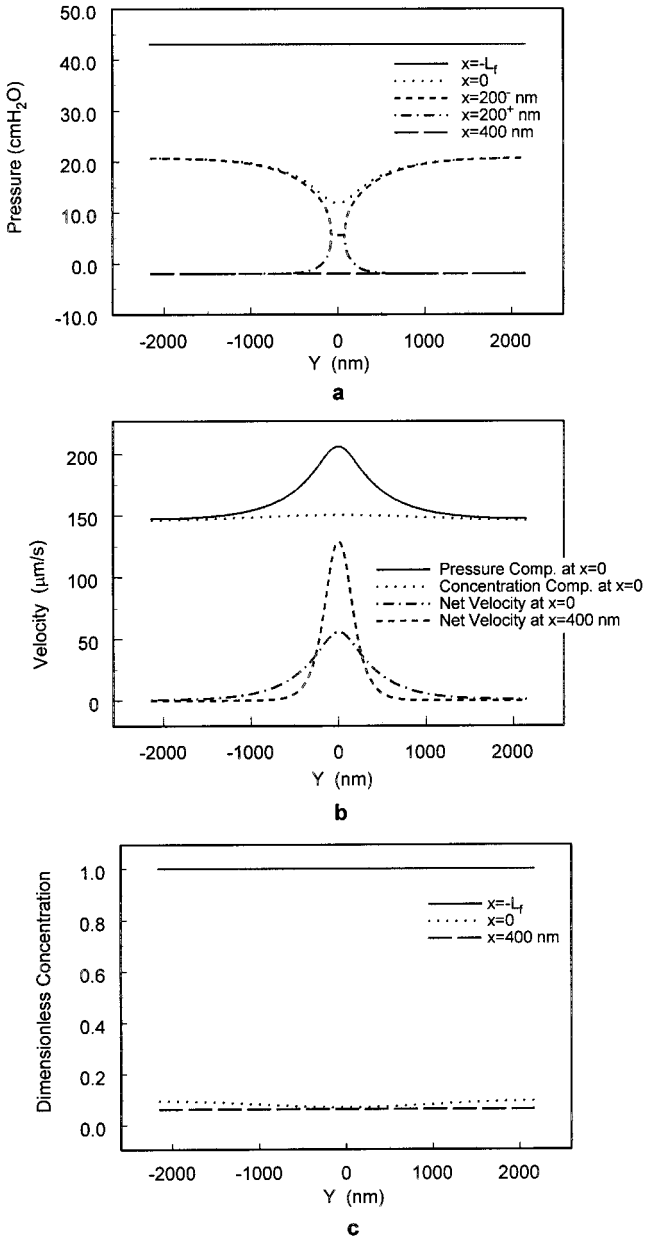

FIG. 3. Predictions of theoretical model for P_c = 43 cm H_2O for the steady-state (a) pressure, (b) velocity, and (c) protein concentration profiles at various locations in cleft identified in Fig. 2. Plasma oncotic pressure is 26 cm H_2O and $\sigma_f = 0.94$. Note that the individual contributions to the water flux crossing the surface glycocalyx from oncotic (protein concentration) and hydrostatic (pressure) components nearly cancel in b except for the region in front of the junction strand break, and the concentration gradients within the cleft are small in c. (a) Roughly half the pressure drop occurs across the matrix and half across the cleft.

constant at −2 cm H_2O as mentioned earlier. The pressure and concentration profiles at $x = 200^-$ and $x = 200^+$ nm have been omitted in Figs. 3c, 4a, 4c, and 5c because these profiles are nearly identical to the profiles at $x = 0$ and $x = 400$ nm, respectively. The detailed concentration profiles in the cleft are shown on an enlarged scale in Fig. 6. The u component of the velocity profiles is shown only at $x = 0$ and 400 nm in Figs. 3b, 4b, and 5b since the u component of the velocity vanishes along the junction strand except at the break. However, more insightful for understanding the osmotic behavior is not the net u component profiles at $x = 0$, but the separate u profiles for the hydraulic pressure and oncotically driven components of the local water flux, because the net u profile is the resultant of these two opposing flow components. Figures 6a and 6b provide a blow-up of the concentration distribution within the cleft, where profiles are shown for $y = 0$, the orifice centerline; $y = 75$ nm, the edge of the orifice, and three other representative values of y along the length of the cleft, $y = 150$, 1080, and 2160 nm, the last corresponding to $y = D$, the half spacing of the neighboring orifices.

(A) High capillary pressure. As shown in Fig. 3a, where P_c = 43 cm H_2O, the pressure drop across the surface matrix layer along the cleft is approximately one-half of the total transendothelial pressure drop except for the region in front of the orifice break in the junction strand. One notes in Fig. 3b that the u profiles at the entrance, $x = 0$, and exit, $x = 400$ nm, are not the same although the junction strand is located at the midpoint of the cleft depth. This differs from our previous model (Fu *et al.*, 1994, 1997) where the hydraulic resistance of the surface matrix was distributed evenly over the entire region, $x < 200$ nm, in front of the junction strand and the profiles were identical. In contrast, if the fiber matrix is treated as a distinct fiber layer in the region, $-L_f < x < 0$, in front of the cleft entrance, the fiber matrix will broaden the velocity profile on the luminal side of the junction strand and reduce the peak velocity at $y = 0$. The streamlines on the tissue side of the junction strand are much more constrained after they pass through the junction orifice and spread to a width at the cleft exit that is approximately three times the width of the orifice opening. The intriguing result for the velocity

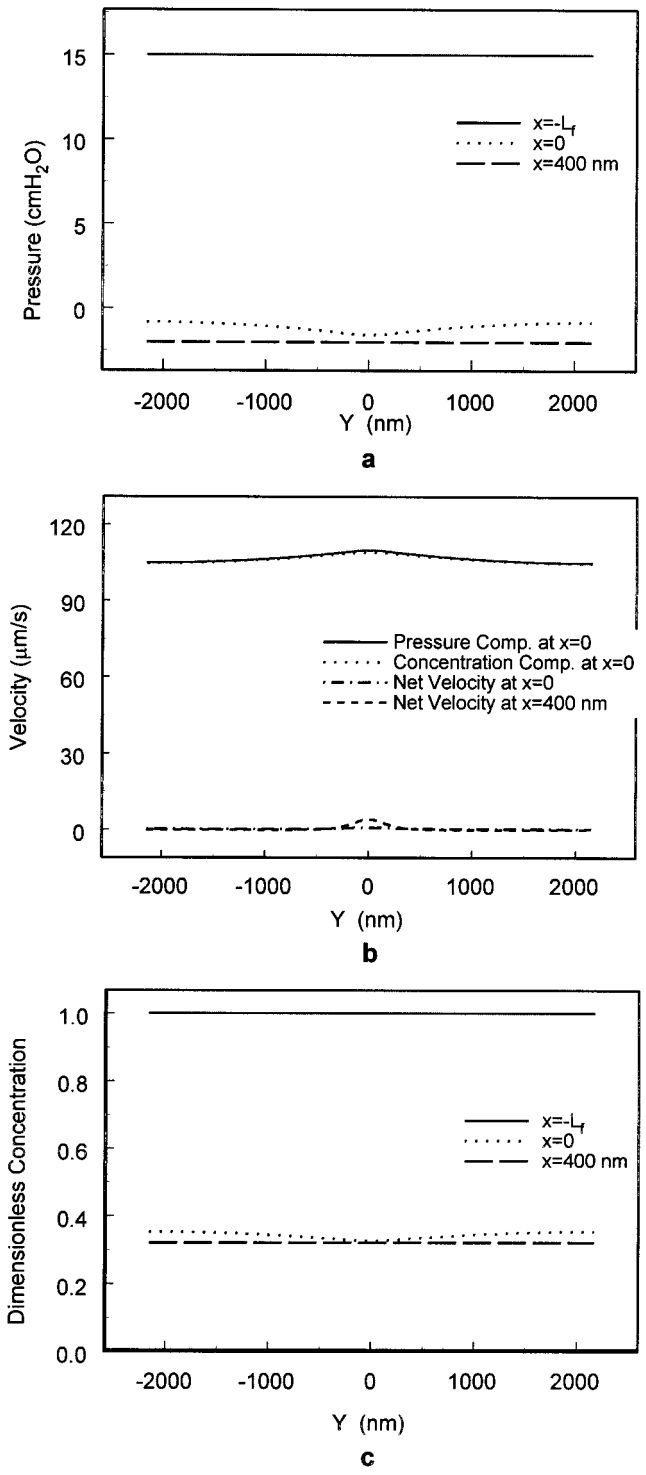

FIG. 4. Predictions of theoretical model for P_c = 15 cm H_2O for the steady-state (a) pressure, (b) velocity, and (c) protein concentration profiles at various locations in cleft identified in Fig. 2. Plasma oncotic pressure is 26 cm H_2O and σ_f = 0.94. Note that the individual contributions to the water flux crossing the surface glycocalyx from oncotic (protein concentration) and hydrostatic (pressure) components cancel everywhere in b leaving only a very small positive filtration in the steady state, and concentration gradients within the cleft are small, as in Fig. 3c. In contrast to Fig. 3a most of the pressure drop occurs across the surface matrix where the pressure and oncotic forces balance one another.

profiles is that the pressure driven component is nearly identically balanced by the osmotically driven component except for the region in the vicinity of the orifice opening, producing a net u profile that vanishes all along the cleft except in this region.

In Fig. 3c, the first surprising result is that the protein concentration at the cleft exit, x = 400 nm, is uniform. Since the velocity profile at x = 400 nm in Fig. 3b has a sharp peak below the orifice in the junction strand, one might expect that more protein will be washed away in this region and the exit concentration reduced. The value of $C_i = J_s/J_v$ proposed by Michel and Phillips (1987) has been applied at the edge of region C, in this case x = 100 μm, yet the protein concentration at x = 400 nm, the cleft exit, differs insignificantly on the scale shown from this value of C_i. This indicates that the protein concentration is uniform in the entire pericapillary region, when the only pathway for transendothelial protein transport is through the cleft. The second surprising result is that the protein concentration varies little within the cleft itself. The concentration profiles at x = 0 and x = 400 nm differ by less than 3% of the plasma concentration at any value of y. The detailed concentration profiles within the cleft for this case are shown in Fig. 6a.

(B) Low capillary pressure, steady state. There are several fundamental differences between the profiles in Fig. 4, where P_c = 15 cm H_2O, and those just described for the high filtration state. The pressure drop across the fiber matrix layer (see Fig. 4a) far exceeds the pressure drop within the cleft itself. The striking result in Fig. 4b is that there is virtually no net water flow across the surface glycocalyx along the entire length of the cleft. The separate contributions of the hydrostatic pressure and the oncotic pressure to the net water flux almost cancel everywhere, includ-

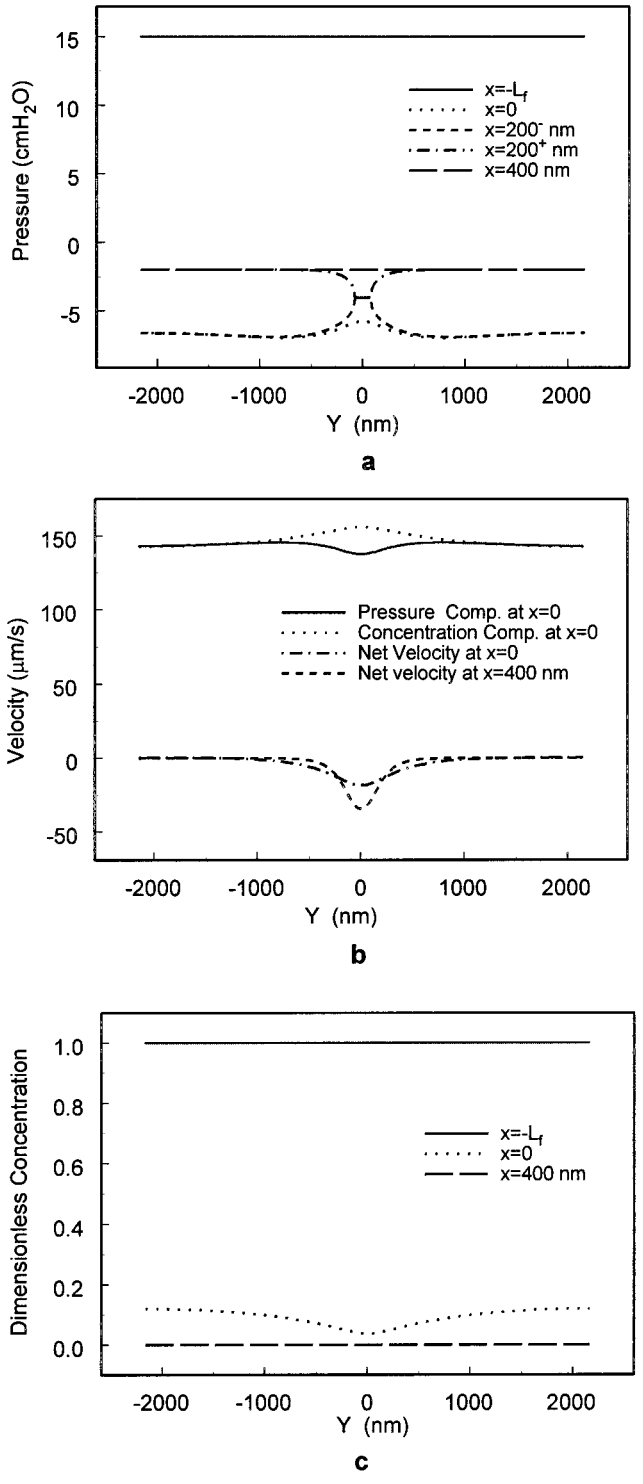

FIG. 5. Predictions of theoretical model for P_c = 15 cm H_2O for transient state (a) pressure, (b) velocity, and (c) protein concentration profiles at various locations in cleft identified in Fig. 2. Plasma oncotic pressure is 26 cm H_2O and σ_f = 0.94. Note that the individual contribution to the water flux crossing the surface glycocalyx from the oncotic component (protein concentration) overrides the hydrostatic (pressure) component over the orifice opening in b, and there is a net negative velocity in the vicinity of the orifice opening. There is a negative pressure of approximately −7 cm H_2O behind the surface matrix, a, and a small standing gradient in concentration is produced across the cleft, c.

ing over the orifice opening. There is no net absorption at any y location, although the hydraulic pressure, 15 cm H_2O, is much lower than the plasma oncotic pressure, 26 cm H_2O. The concentration at the cleft exit has now risen to a value that is 32% of the plasma concentration, but the concentration gradient within the cleft is again remarkably small as shown in detail in Fig. 6b, where one observes that the concentration varies by less than 1% of the plasma concentration along the orifice centerline at $y = 0$. Nearly the entire concentration gradient is experienced across the surface glycocalyx, as in the high filtration state, but this time the oncotic force is sufficient to balance the filtration pressure everywhere. The pressure drop within the cleft, Fig. 4a, is greatly diminished because the net filtration velocity u has nearly vanished everywhere.

(C) Low capillary pressure, transient state. In the case of the transient flow with P_c = 15 cm H_2O, we assume that the pressure is suddenly decreased from 43 to 15 cm H_2O and there is insufficient time for the tissue concentration to change from a preexisting condition in which a high flow of protein-free perfusate washes over the tissue. Thus, we assume that the concentration at the cleft exit is zero. The intriguing result in Fig. 5a is that the pressure inside that the cleft is negative everywhere and lower than that at the cleft exit, −2 cm H_2O. The pressure at $x = 0$ just behind the fiber matrix is nearly −7 cm H_2O and rises slightly above the orifice opening. This negative pressure gradient is required to suck fluid from the tissue through the cleft before it can be absorbed across the surface glycocalyx into the capillary, as is clearly shown in Fig. 5b. The oncotic pressure difference across the surface matrix layer, about 22 cm H_2O, exceeds the hydrostatic pressure drop across the surface layer, especially in the vicinity of the orifice opening, and

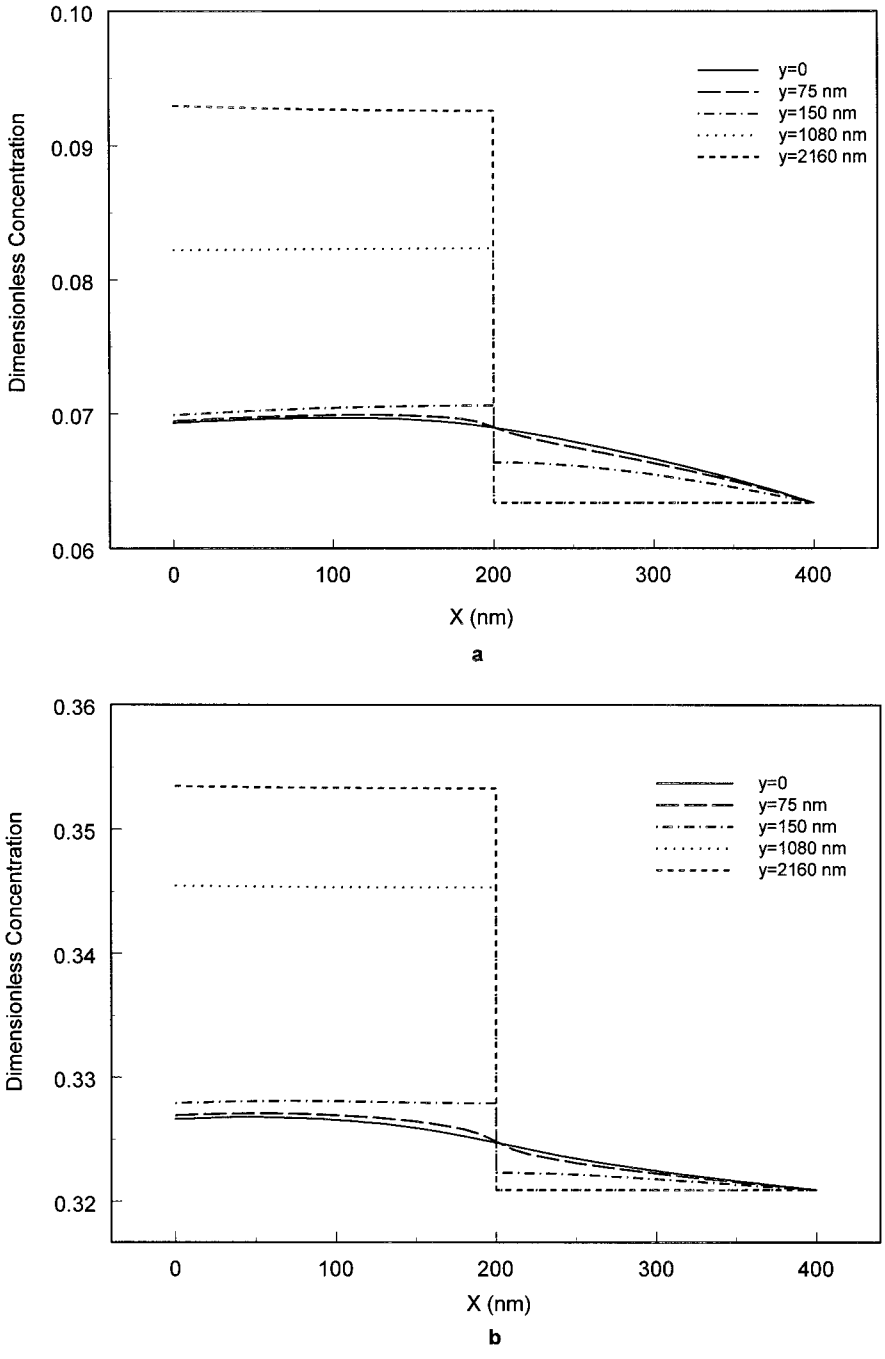

FIG. 6. Predictions of the theoretical model for the dimensionless concentration profiles within the cleft at different y locations for (a) P_c = 43 cm H_2O and (b) P_c = 15 cm H_2O. $C_i = J_s/J_v$ is applied at the end of region C, x = 100 μm. y = 0, centerline; y = 75 nm, edge of orifice; y = 2160 nm, half spacing of junction strand breaks. Other conditions are the same as those in Figs. 3 and 4.

there is negative velocity at $x = 0$ and $x = 400$ nm in the neighborhood of the breaks in the junction strand. The solute concentration within the cleft behind the surface matrix layer has adjusted such that the total oncotic pressure across this layer has nearly canceled the net hydrostatic difference (15 cm H_2O minus -7

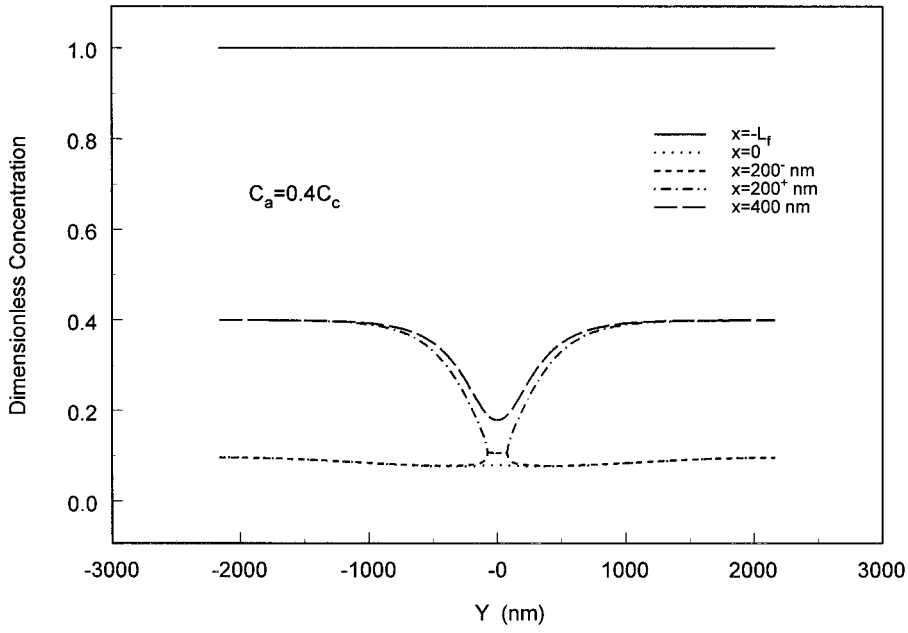

FIG. 7. Concentration profiles in the cleft when P_c = 43 cm H_2O and there is a parallel nonconvective pathway for albumin which increases the tissue concentration at the edge of region B, C_a, to 0.4C_c. Flow geometry is shown in Fig. 2. Plasma oncotic pressure is 26 cm H_2O and σ_f = 0.94. Note that the profile behind the surface matrix, at $x = 0$, is nearly the same as the concentration profile at $x = 0$ in Fig. 3c.

cm H_2O or 22 cm H_2O) except in the vicinity of the orifice opening. Note once again that the net water flux vanishes everywhere except over the orifice.

2. *Analysis of Parallel Large Pore Pathway*

Figures 3 and 4 describe conditions where the entire protein flux passes through the interendothelial cleft and an equilibrium state $C_i = J_s/J_v$ is established somewhere in the tissue space. In addition to the breaks in the cleft, a large nonselective pore may also contribute to protein transport. This pore can take the form of active vesicle transport, channels of fused vesicles, or transient gaps in an inflammatory response (Michel, 1997). Thus, in Fig. 7 we have shown the model predictions for the concentration profiles that would result if there is a parallel nonselective pathway for proteins, which would raise the concentration at the edge of region B to 0.4C_c, a typical value for mammalian capillaries (Levick, 1991). All other conditions are the same as those shown in Fig. 3 where the capillary pressure P_c = 43 cm H_2O. This new value of C_a in the tissue space, which is more than six times the value of $C_i = 0.063C_c$, shown in Figs. 3c and 6a, is due to the superposition of two fluxes, one through the cleft and a transcellular flux. The remarkable result is that there is little change in the protein concentration profile at $x = 0$, just behind the surface matrix layer in Fig. 7, and the corresponding profile in Fig. 3c, although there are now large concentration gradients within the cleft on the tissue side of the junction strand, at the cleft exit, and in the pericapillary space as observed in Figs. 8a and 8b. The concentration in the protected region, $0 < x < 200$ nm, is very close to the predicted value for the convective limit, $C = (1 - \sigma_f)C_c$. This striking new predication will be explained in the Discussion.

Figure 8a shows both the cleft region A and the exit mixing region B, while Fig. 8b is a blow-up of just region A to elucidate the important difference in behavior upstream and downstream of the junction strand. Because the concentration profiles at $x = 0$ are almost unaltered, the pressure and velocity profiles are nearly the same as shown in Figs. 3a and 3b. Note that the protein concentration at the cleft exit is nonuniform and has a value close to that at the edge

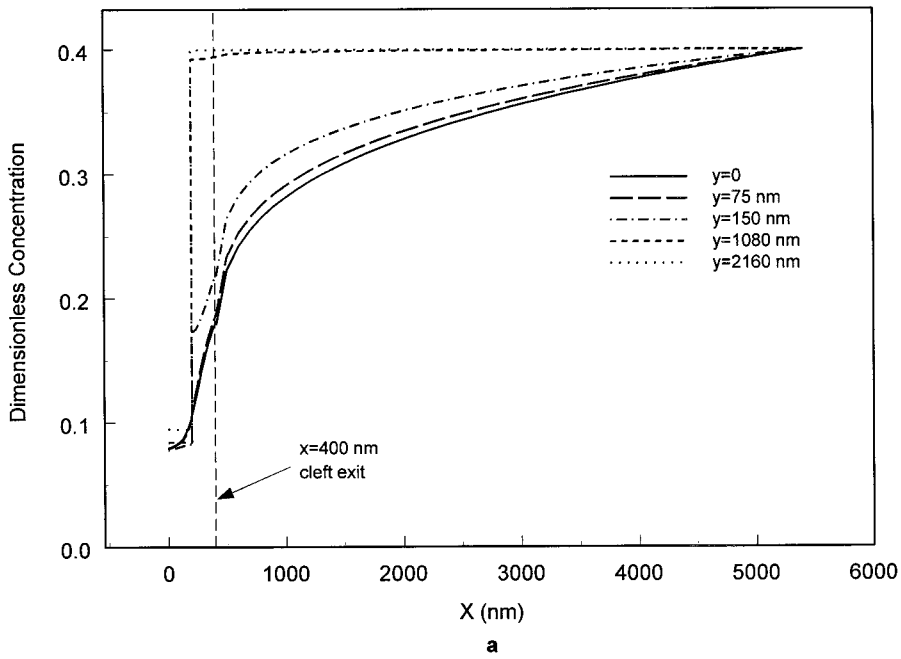

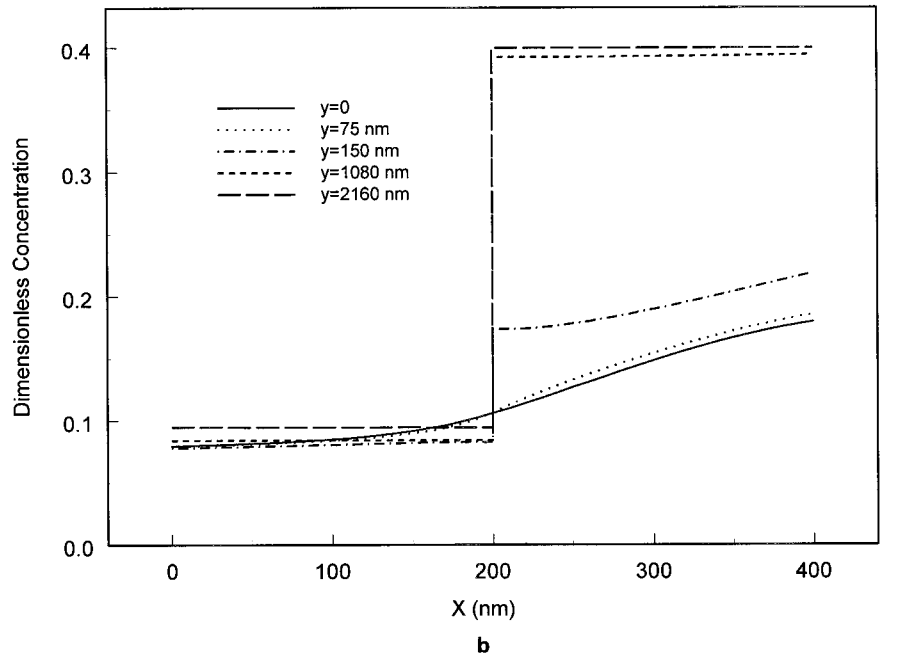

FIG. 8. Predictions of the theoretical model for the dimensionless concentration profiles at different y locations for (a, b) P_c = 43 cm H_2O and (c) P_c = 15 cm H_2O when there is a parallel nonselective pathway for protein which increases the tissue concentration at the edge of region B, C_a, to $0.4C_c$. (a) Upstream spread of solute from the pericapillary region B into the cleft; (b, c) Detailed profiles within the cleft corresponding to Figs. 6a and 6b, where the entire flux is through the cleft and there is no parallel pathway.

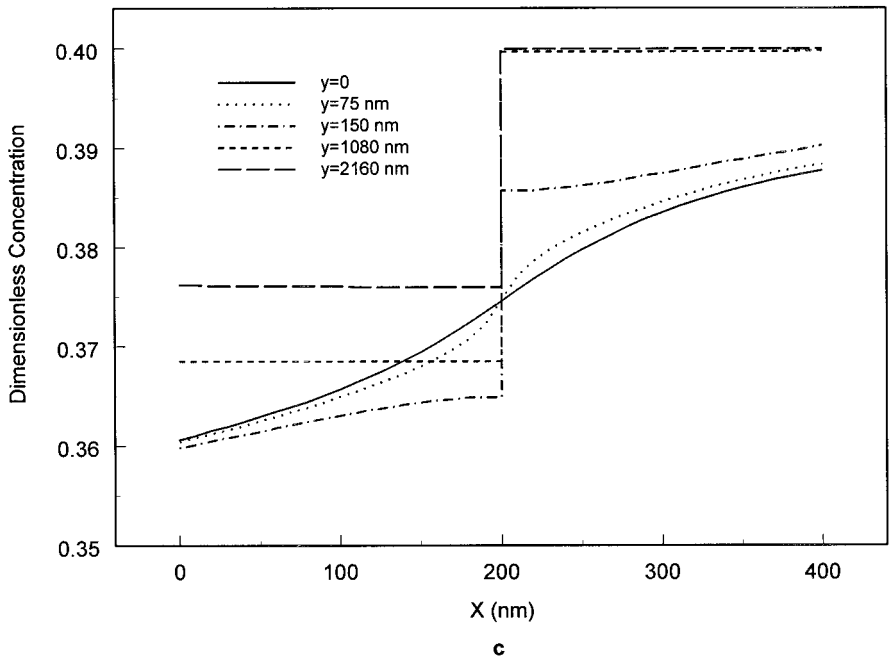

FIG. 8—*Continued*

of region B, except the vicinity of the orifice opening, where the fluid flow washes the protein away and dilutes the solute concentration, a result similar to that observed for fenestrated capillaries (Levick, 1994). The solute profiles in the cleft at low capillary pressures, P_c = 15 cm H_2O, are shown in Fig. 8c. In this case the net filtration is very low and the back diffusion into the cleft is more significant, even upstream of the junction strand. This back diffusion at low capillary pressures will be reduced if there are some matrix components in the cleft and the diffusion coefficient in the cleft, D_c, is decreased.

The curves in Fig. 9 for $C_a = 0.4C_c$ clearly shows the dramatic difference in the net filtration predicted using the classical application of Eq. (1), where the Starling forces are based on the global transendothelial difference in concentration and pressure between the plasma and tissue space, and the present spatially heterogeneous model where the oncotic and pressure forces are due to the local concentration and pressure differences across the surface matrix layer. Results are shown for two values of D_c, D_∞ and a value which is the same as in the tissue, $0.13D_\infty$. In the global model, the fluid flux per unit area through the capillary wall is calculated from Eq. (1) using the same hydraulic permeability L_p as in our spatially heterogeneous model. One observes that the new model predicts a marked reduction in filtration, which is especially significant for the lower value of D_c, when the capillary pressure is less than the plasma oncotic pressure. For this lower value of D_c the reduction in flux is more than a factor of 5 when $P_c < 20$ cm H_2O. The large difference between the predictions of Eq. (1) and the new model is largely due to the fact that the protein concentration behind the surface matrix layer is far lower than in the tissue space as already noted in Figs. 7 and 8.

Figure 9 also shows the predictions for Michel and Phillips' experiment where all the solute transport is assumed to pass through the cleft. The difference between the dot–dash–dot curve, $C_a = 0.4C_c$, and the dashed curve, $C_a = J_s/J_v$, for $D_c = D_\infty$ is due to back diffusion from the tissue space when $C_a = 0.4C_c$. The dashed curve thus provides a lower limit for the fluid flux when the nonselective parallel pathway is removed.

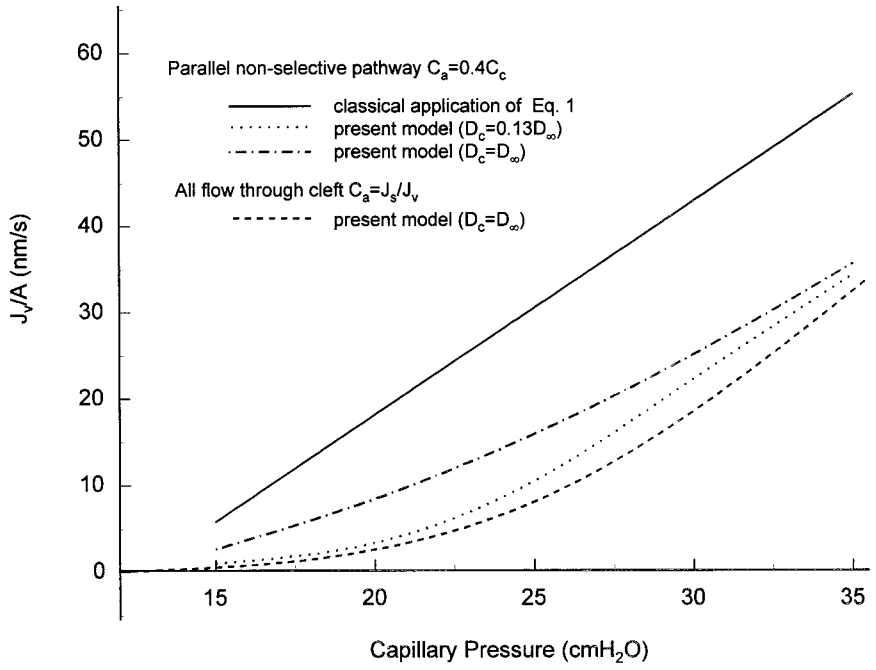

FIG. 9. The comparison of the filtration flux, J_v/A, predicted by the present model and the classical application of the Starling equation when $C_a = 0.4C_c$ and $\pi_c = 26$ cm H_2O. According to classical theory, where P_i and π_i are evaluated in the tissue space, J_v/A varies linearly with capillary pressure P_c. In the present model, where P and π are evaluated locally across surface matrix layer, the filtration flow is highly nonlinear and greatly reduced. The water flow through the junction strand orifice impedes the back diffusion of solute in the tissue from entering the protected region behind the surface matrix. This effect is significantly enhanced if the diffusion coefficient in the cleft D_c is reduced to a value $0.13D_\infty$ representative of matrix components in the tissue space. Also shown for comparison are the results that would be obtained if the entire solute flux were through the cleft and $C_a = J_s/J_v$. $D_f = 0.001D_\infty$ in all cases.

3. *Effect of D_f on Filtration–Pressure Curve*

Figure 10 shows the effect of the diffusivity of the surface matrix layer, D_f, on the filtration–pressure curve. Also shown is the transient response when the tissue is bathed in a protein-free perfusate and the protein concentration at the cleft exit is zero. As Michel and Phillips (1987) predicted, in the transient state there is absorption at low capillary pressures and one obtains a classic Landis–Starling response. This transient response is nearly independent of D_f for $D_f < 0.001D_\infty$ and changes only with the osmotic reflection coefficient, whose value has been fixed at $\sigma_f = 0.94$ for all curves in Fig. 10. The other four curves correspond to different values of D_f in the surface matrix layer. The bend in the curves for J_v vs P_c at steady state becomes more abrupt as D_f is decreased. As D_f decreases, the osmotic force across the surface matrix layer is increased since less solute can diffuse across the surface glycocalyx into the cleft. This leads to a decrease in fluid flux since the oncotic force for absorption is increased. As noted in the section on parameter values, there is no adequate theory for predicting D_f when the solute size approaches the fiber spacing. However, the results in Fig. 10 provide a means for estimating D_f. One observes that there is excellent agreement with Michel and Phillips' (1987) experiment when D_f lies in the range 0.001 to $0.0001D_\infty$. This suggests a surface matrix that is a formidable barrier to Ficoll 70 with a diffusion coefficient that is three orders of magnitude smaller than the free diffusion coefficient and a reflection coefficient that is close to 1. Again, this value of D_f relates only to the cleft pathway. The total measured value of the permeability also includes transcellular transport due to vesicles and transient gaps.

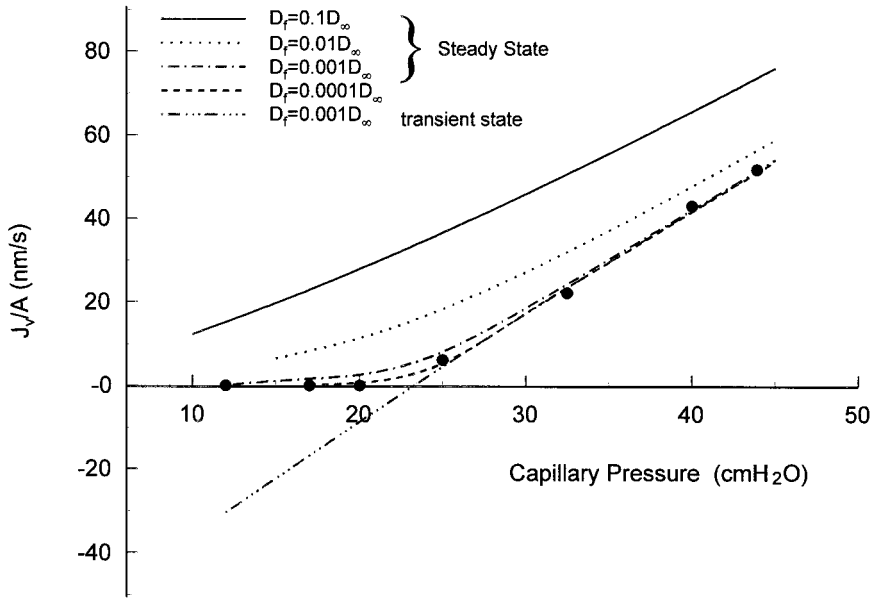

FIG. 10. The relation between filtration flux, J_v / A, and capillary pressure, P_c, for different diffusion coefficients, D_f, of the surface matrix layer in both the steady and transient states. Plasma oncotic pressure is 26 cm H_2O and interstitial hydraulic pressure is zero. The filled circles (●) are the measured values from Michel and Phillips (1987). Note the close agreement between theory and experiment when D_f lies between 0.001 and $0.0001D_\infty$.

DISCUSSION

The motivation for this study was the outgrowth of lengthy discussions between the senior author and J. R. Levick and C. C. Michel at the 1996 Starling Symposium. These discussions centered around four fundamental questions: (A) the spatial heterogeneity of the water and solute fluxes across the surface matrix layer; (B) the appropriate boundary conditions that should be applied in the tissue space; (C) how the solute concentration profiles behind the surface matrix layer were related to the tissue protein concentration if there were nonselective transcellular pathways for protein across the endothelium, and (D) how the classic Starling equation should be applied, globally across the entire endothelial layer or locally across the protein sieving layer at the endothelial surface if the primary sieving layer is the surface glycocalyx. We will first address each of these basic questions.

A. Spatial Heterogeneity of the Filtration Flux and Oncotic Force

In view of the large spatial variation in the local water flux crossing the surface glycocalyx (see Figs. 3b, 4b, and 5b), one might anticipate that there are large spatial gradients in the albumin concentration behind the surface matrix layer and consequently large gradients in the local oncotic force. In fact, we initially expected, based on the one-dimensional model of Michel and Phillips (1987), that where the water flux was low in regions removed from the junction strand breaks, the albumin concentration would approach that in the plasma (the diffusion limit), whereas over the orifice opening, where the water flux was high, the concentration would approach the limiting value, $(1 - \sigma_f)C_c$, predicted for the convective limit. However, the solutions presented in Figs. 3c, 4c, and 5c show, surprisingly, that the protein concentration profiles at $x = 0$ have only a minor variation. This same behavior is observed whether there is filtration, Figs. 3c and 4c, or absorption, Fig. 5c.

In general, the detailed concentration profiles in Fig. 6 for Michel and Phillips' experiment reveal that there are only small gradients in concentration throughout the cleft as intuitively argued by Michel (1997). In the case where the tissue concentration is elevated by the inclusion of a parallel large pore pathway, Fig. 8b, larger gradients appear on the tissue side of the junction strand, but the gradients in the protected region on the lumen side of the junction strand are comparable to those shown in Fig. 6a. These observations indicate that there will be only small solute gradients behind the surface matrix layer provided that the junction strand serves as an effective diffusive barrier and the diffusion coefficient in the cleft $D_c \gg D_f$.

The fluid streamline pattern and y-direction velocity profiles exhibit a much greater spatial heterogeneity than the concentration profiles just described. This is because the cleft and the junction strand play a much more important role in determining the pressure distribution across the endothelial layer. In contrast to solute transport, a significant fraction of the total transendothelial pressure drop occurs across the cleft itself when there is a significant water flux. This is true for steady state filtration, Fig. 3a, or transient absorption, Fig. 5a. Due to this pressure distribution, the u profiles at $x = 0$ and, therefore, the fluid streamlines, are concentrated in the vicinity of the orifice opening in the junction strand as shown in Figs. 3b and 5b.

B. Boundary Conditions in the Tissue Space

A central question in formulating the model and interpreting its results is the boundary condition in the tissue space. Starling in his original paper (1896) realized that the protein concentration in the tissue space depended on the flux of solute into the tissue. Michel and Phillips (1987) proposed that this equilibrium solute concentration is given in the steady state by the ratio of two fluxes, J_s to J_v. The condition $C_i = J_s/J_v$ is appropriate only if the solute in the tissue is well mixed and uniform. The question as to how this uniformity is achieved is never addressed.

In the present model we have not assumed *a priori* that Michel's condition, $C_i = J_s/J_v$, applies at the cleft exit, since we wanted to leave open the possibility that the solute flux is nonuniform along the length of the cleft exit. Instead, we have required that the concentration at the edge of region B first achieve a uniform value C_a and then allow for further mixing in region C, before achieving the final well-mixed condition, $C_i = J_s/J_v$. This condition was applied at different distances from 5 to 100 μm into the tissue. The results for Michel and Phillips' experiment were insensitive to the size of region C. One finds that both regions B and C are, indeed, uniform when all the solute enters along with the water through the cleft. The entire tissue space does act like a well-mixed reservoir, as proposed by Michel and Phillips (1987), provided, as we shall discuss next, that there is not a parallel large pore pathway.

Suppose now that the tissue concentration at the edge of region B, C_a, is elevated by a flux through a large pore, transcellular nonconvective pathway removed from the cleft, but region C is well mixed and uniform. This requires that $C_a > J_s/J_v$, where J_s and J_v are still the solute and water fluxes through the cleft. The ratio of the prescribed value of C_a, in this case $0.4C_c$, to the value obtained from the expression, $C_i = J_s/J_v$, also represents the ratio of solute flux through all pathways to the solute flux through the cleft pathway in the steady state, if the local tissue region is at uniform concentration. Thus, in the convective limit, where $C_i = (1 - \sigma)C_c$, one finds that the solute flux through the large pore pathway is nearly six times that through the cleft, if $\sigma = 0.94$, and region B is highly nonuniform in contrast to the results for Michel and Phillips' experiment. The intriguing result, which we shall now examine in more detail, is that the model predicts that one can substantially change the concentration in the tissue space without significantly changing the solute concentration on the lumen side of the junction strand. This has very important implications for the application of the Starling equation.

C. Large Pore Parallel Pathway

The results in Figs. 7 and 8 show that when the protein concentration is elevated in the pericapillary space at the edge of region B due to a parallel large pore, nonconvective pathway, large solute gradients are produced in the region downstream of the cleft exit. As observed in Fig. 8, the solute gradients feed upstream into the cleft. The important observation is

that the large elevation in concentration that occurs in the tissue and in the cleft downstream of the junction strand is not communicated upstream through the orifice opening at the high capillary pressure (Figs. 8a and 8b). The region between the surface matrix layer and the junction strand is effectively insulated from the conditions in the tissue.

To examine the role of the orifice more carefully we have calculated the ratio of the convective to the diffusive flux of the solute at the orifice opening for the conditions shown in Fig. 8b. Convection was 47 times greater than diffusion and the local Peclet number based on the cleft depth, 400 nm, and centerline velocity was 4.7. The orifice thus acts at high capillary pressures like a throat that prevents the back diffusion of solute into the shielded region in front of the junction strand. The oncotic pressure behind the surface glycocalyx is effectively uncoupled from the oncotic pressure in the tissue when the convective flux through the orifice opening dominates diffusion at this critical cleft location. Only for conditions of very low filtration will the tissue concentration significantly influence conditions behind the surface matrix layer. This is observed in Fig. 8c where the cleft solute profiles are shown for $P_c = 15$ cm H_2O. The dimensionless concentration has risen to a value that is roughly 90% of that in the tissue space. The local Peclet number is now only 0.15 and the profiles on each side of the orifice opening are more symmetric indicating that solute diffusion now plays an important role.

In the present paper the edge of region B has been prescribed. It has been estimated on the basis of anatomical data to be 5 μm, half the average cleft spacing. One observes in Fig. 8a that the solute gradient is greatly diminished, but does not vanish at the edge of region B, $L_B = 5$ μm. This implies that, according to the present model, the solute concentration is not uniform in region C, but only nearly so. A more sophisticated model is needed to more accurately describe the details of the mixing between the paracellular cleft and transcellular large pore or vesicular pathways.

D. Application of the Starling Equation

The Starling equation has heretofore been universally applied to the global differences in protein concentration and pressure between the plasma and the tissue space. The present model is based on a new hypothesis, that the oncotic and hydrostatic pressures, π_i and P_i, must be applied locally to only that portion of the endothelial barrier where we hypothesize that the proteins are actually being sieved, namely, the surface matrix layer. This hypothesis leads to two fundamental changes in current thinking. First, the local Starling forces are spatially heterogeneous on the length scale of the spacing between junction orifices because of the large variation in local Peclet number as noted in subsection A. Second, the local protein concentration and pressure behind the surface matrix layer can differ greatly from the tissue concentration and pressure.

Our model predicts that the cleft itself is able to support only minor concentration gradients when the exit condition, $C_i = J_s / J_v$, is satisfied. Michel's simple, one-dimensional model thus provides a reasonable estimate of the protein concentration in the tissue when the entire solute flux passes through the cleft, since the solute gradients across the cleft are small compared to those across the matrix layer and the concentration behind the matrix is well approximated by C_i. The pressure at the rear of the surface matrix layer, on the other hand, can differ greatly from the pressure in the tissue if the primary pressure drop occurs across the junctional strand, as observed in Fig. 3a.

The fact that the pressure and concentration behind the surface glycocalyx can differ greatly from their values in the tissue means that the Starling forces across the matrix layer will depart significantly from the global Starling forces across the entire endothelial layer. This can lead to drastically different results for the filtration flow as shown in Fig. 9. This difference will be particularly important in the case where there is a parallel, large pore solute pathway across the endothelium, since the oncotic pressure behind the surface matrix layer can be nearly independent of the tissue concentration, as is evident in Fig. 8b. However, even in the case where the entire water and solute flux is through the cleft, the Starling forces at the back of the matrix and in the tissue space will not be the same. The oncotic forces will differ by only a few percent, because the solute gradients in the cleft are small, but

the pressure forces can differ greatly as noted at the end of the previous paragraph.

E. The Surface Glycocalyx and Other Matrix Structures

The basic hypothesis in our new conceptual mathematical model is that the surface glycocalyx is both the primary molecular sieve and diffusive barrier for plasma proteins and that this sieving matrix does not fill the entire interendothelial cleft as proposed in the original fiber matrix theory of Curry and Michel (1980). At present the evidence for this is only indirect since the matrix is not electron dense and, therefore, not easily observed. The most convincing evidence that the sieving structure is confined to a surface layer is the detailed calculations for L_p for frog mesentery of Fu *et al.* (1994), the measurements of the surface matrix layer thickness for this microvessel (Adamson and Clough, 1992), and the recent theory and experiments for the labeling of the cleft using high-molecular-weight tracers (Fu *et al.*, 1997, 1998). A rigorous hydrodynamic theory has been developed by Tsay and Weinbaum (1991) for the hydraulic resistance of cleft-spanning fibers in a channel. This theory has been used (Fu *et al.*, 1994) to estimate L_p in frog mesentery using the measured structure of the junction strands of Adamson and Michel (1993) that has been applied in the present model. These quantitative predictions show that the measured L_p of $2.0*10^{-7}$ cm/s/cm H_2O would be underpredicted by at least a factor of 4 if a sieving matrix for albumin with a fiber spacing of 7 nm were to fill the wide part of the cleft. The predicted thickness of the matrix layer of Fu *et al.* (1994), 100 nm, was nearly the same as the measured thickness of the surface matrix layer of Adamson and Clough (1992). The latter was indicated by a dense band of cationized ferritin (11-nm diameter) that was displaced from the endothelial surface. The serial section electronmicrographs of Adamson and Michel (1993) clearly reveal that the gap height of the breaks in the junction strand, 20 nm, is essentially the same as the wide part of the cleft. Thus, the junction strand itself is unlikely to provide the molecular sieve for plasma proteins. This combined evidence has led the authors in recent publications (Fu *et al.*, 1994, 1997; Weinbaum, 1998) and Michel (1997) to hypothesize that the surface glycocalyx is the molecular filter, at least for frog mesentery capillaries.

Additional evidence in support of the hypothesis that the surface matrix does not also fill the cleft comes from the theoretical predictions of Fu *et al.* (1997) and the recent unpublished experimental observations of R. Adamson for the labeling of the cleft using a high-molecular-weight tracer, horseradish peroxidase (HRP). In early experiments using HRP in pure Ringer, one would frequently see HRP penetrating the cleft up to the level of the junction strand and an occasional leakage of HRP which would extend throughout the depth of the cleft. However, the more recent studies of Adamson and Clough (1992) reveal that the surface matrix collapses in the absence of plasma proteins. When the HRP tracer experiment is performed *ex vivo* in frog mesentery, where the surface matrix is intact, there is no detectable filling of the cleft (R. Adamson, private communication). If the matrix were to fill the cleft, one would expect to see a linear decrease in peroxidase reaction product with distance into the cleft, which does not occur. The theoretical model of Fu *et al.* (1997) explains these observations by showing that even in the vicinity of a junction strand break, the concentration of HRP behind the surface matrix would be so reduced that its reaction product would not be visible. Thus, in contrast to the tracer labeling studies with the low-molecular-weight tracer, lanthanum (Adamson and Michel, 1993), one would not expect to see HPR reaction product in the cleft, if there was a sieving matrix at the endothelial surface.

F. Is There a Need for Venous Reabsorption?

Figure 9 shows that even if the tissue concentration is raised to $0.4C_c$ the filtration on the arterial side is far smaller than previously believed and significantly less than the solid line in Fig. 9, where the Starling forces are based on global values of the pressure and concentration in the tissue. Based on the results in Fig. 9, there may be no need for venous reabsorption because the net filtration is much less than that predicted by a classical Landis–Starling diagram in which both P and π are based on their interstitial values. The magnitude of the reduction in the net filtration depends on how

effective the junction strand is in preventing back diffusion from the tissue space. The critical parameter is the magnitude of the Peclet number evaluated at the junction strand orifices. When Pe $>$ 1 the concentration in the protected region behind the matrix layer is effectively uncoupled from that in the tissue space. The actual reduction in net filtration is not the difference in area under the curves in Fig. 9 although this provides a rough guide. One needs to examine the permeability-area distribution of the capillary and it is well recognized that capillaries on the venous side have a significantly larger area. This weights the venous end of the capillary where the model predicts that the filtration rate is very low.

An important issue that has not been addressed is what happens in more restrictive transport barriers in mammalian capillaries and other tissues where there are multiple junction strands and much lower hydraulic conductivities. The serial sections in rat heart capillaries (Bundgaard, 1984) suggest that the junction strand breaks are both much shorter, typically one section thickness, 400–500 nm, and more widely spaced. While these more complicated junction structures are beyond the scope of the present paper, it is anticipated that the same basic principle applies. For widely dispersed small pores L_p will be greatly decreased, but the small filtration flux will need to be funneled through a reduced population of small pores with the net result that the Peclet number at the junction orifices is not greatly different from the values predicted herein for frog mesentery. If this is the case the rear of the surface matrix would be shielded from back diffusion from the tissue and the effective oncotic pressure uncoupled from the tissue concentration as demonstrated for frog mesentery in the present study.

APPENDIX

In this Appendix the expression of the steady-state protein concentration in the tissue far from the cleft exit is derived for the case where the entire solute flux is through the cleft. The protein concentration in the steady state is equal to ratio of the total solute flux J_s to the total fluid flux J_v. From continuity, these two fluxes are identical at every cross-section for steady-state conditions. For convenience, we evaluate J_s and J_v at $x = 0$, the cleft entrance. The local fluxes j_s and j_v can be written as

$$j_s(y) = \frac{D_f}{L_f}[C_c - C(0, y)]\frac{\mathrm{Pe}}{e^{\mathrm{Pe}} - 1} + \tfrac{2}{3}C_c(1 - \sigma_f)u_0(0, y), \quad \text{(A1)}$$

$$j_v(y) = \tfrac{2}{3}u_0(0, y), \quad \text{(A2)}$$

where

$$\mathrm{Pe} = \frac{j_v(1 - \sigma_f)L_f}{D_f}.$$

Total solute and fluid fluxes across each cross-section of the cleft are

$$J_s = 2h\int_{-D}^{D} j_s(y)dy, \quad \text{(A3)}$$

$$J_v = 2h\int_{-D}^{D} j_v(y)dy, \quad \text{(A4)}$$

and the expression for C_i is given by

$$C_i = \frac{\int_{-D}^{D}\left[\frac{D_f}{L_f}(C_c - C(0, y))\frac{\mathrm{Pe}}{e^{\mathrm{Pe}} - 1} + \tfrac{2}{3}C_c(1 - \sigma_f)u_0(0, y)\right]dy}{\tfrac{2}{3}\int_{-D}^{D} u_0(0, y)dy}. \quad \text{(A5)}$$

ACKNOWLEDGMENTS

This research is supported by NIH Grant HL 44485 and a Whitaker Foundation sponsored Center for Biomedical Engineering Fellowship to Xiaping Hu. The authors also acknowledge very helpful discussions with Roger Adamson, Fitz-Roy Curry, J. Rodney Levick, and C. Charles Michel.

REFERENCES

Adamson, R. H., and Clough, G. (1992). Plasma proteins modify the endothelial cell glycocalyx of frog mesenteric microvessels. *J. Physiol.* **445,** 473–486.

Adamson, R. H., and Michel, C. C. (1993). Pathways through the intercellular clefts of frog mesenteric capillaries. *J. Physiol* **466,** 303–327.

Bundgaard, M. (1984). The three-dimensional organization of tight junctions in a capillary endothelium revealed by serial-section electron microscopy. *J. Ultrastruct. Res.* **88,** 1–17.

Curry, F. E., and Michel, C. C. (1980). A fiber matrix theory of capillary permeability. *Microvasc. Res.* **20,** 96–99.

Fox, J. R., and Wayland, H. (1979). Interstitial diffusion of macromolecules in the rat mesentery. *Microvasc. Res.* **18,** 255–276.

Fu, B. M., Adamson, R. H., and Curry, F. E. (1998). Test of a two pathway model for small solute exchange across capillary wall. *Am. J. Physiol.* **274** (Heart 43), H2062–H2073.

Fu, B. M., Curry, F. E., Adamson, R. H., and Weinbaum, S. (1997). A model for interpreting the tracer labeling of interendothelial clefts. *Ann. Biomed. Eng.* **25,** 375–397.

Fu, B. M., Tsay, R., Curry, F. E., and Weinbaum, S. (1994). A junction-orifice-entrance layer model for capillary permeability: Application to frog mesenteric capillaries. *ASME J. Biomech. Eng.* **116,** 502–513.

Ganatos, P., Weinbaum, S., Fischbarg, J., and Liebovyitch, L. (1981). A hydrodynamic theory for determining the membrane coefficients for the passage of spherical molecules through an intercellular cleft. *Adv. Bioeng.* **3,** 193–196.

Guyton, A. C. (1963). A concept of negative interstitial pressure based on pressures in implanted perforated capsules. *Circ. Res.* **12,** 399–414.

Guyton, A. C., and Lindsey, A. W. (1959). Effect of elevated left atrial pressure and decreased plasma protein concentration on the development of pulmonary edema. *Circ. Res.* **7,** 649–657.

Levick, J. R. (1991). Capillary filtration–absorption balance reconsidered in light of dynamic extravascular factors. *Exp. Physiol.* **76,** 825–857.

Levick, J. R. (1994). An analysis of the interaction between interstitial plasma protein, interstitial flow, and fenestral filtration and its application to synovium. *Microvasc. Res.* **47,** 90–125.

McDonald, J. N., and Levick, J. R. (1993). Effect of extravascular plasma protein on pressure–flow relations across synovium in anaesthetized rabbits. *J. Physiol.* **465,** 539–559.

Michel, C. C. (1984). Fluid movements through capillary walls. *In* "Handbook of Physiology. Section 2: The Cardiovascular System" (E. M. Renkin and C. C. Michel, Eds.). pp. 375–409. American Physiological Society, Bethesda, MD.

Michel, C. C. (1997). Starling: The formulation of his hypothesis of microvascular fluid exchange and its significance after 100 years. *Exp. Physiol.* **82,** 1–30.

Michel, C. C., and Phillips, M. E. (1987). Steady-state fluid filtration at different capillary pressures in perfused frog mesenteric capillaries, *J. Physiol.* **388,** 421–435.

Perl, W., Chowdhury, P., and Chinard, F. P. (1975). Reflection coefficients of dog lung endothelium to small hydrophilic solutes. *Am. J. Physiol.* **228**(3), 797–809.

Starling, E. H. (1896). On the absorption of fluids from the convective tissue spaces. *J. Physiol.* **19,** 312–326.

Taylor, A. E., and Townsley, M. I. (1987). Evaluation of the Starling fluid flux equation. *News Physiol. Sci.* **2,** 48–52.

Tsay, R., and Weinbaum, S. (1991). Viscous flow in a channel with periodic cross-bridging fibers of arbitrary aspect ratio and spacing. *J. Fluid Mech.* **226,** 125–148.

Tsay, R., Weinbaum, S., and Pfeffer, R. (1989). A new model for capillary filtration based on recent electron microscopic studies of endothelial junctions. *Chem. Eng. Commun.* **82,** 67–102.

Vink, H., and Duling, B. R. (1996). Identification of distinct luminal domains for macromolecules, erythrocytes, and leukocytes within mammalian capillaries. *Circ. Res.* **79,** 581–589.

Weinbaum, S. (1998). 1997 Whitaker distinguished lecture: Models to solve mysteries in biomechanics at the cellular level; a new view of fiber matrix layers. *Ann. Biomed. Eng.* **26,** 1–17.

Weinbaum, S., Tray, R., and Curry, F. E. (1992). A three-dimensional junction-pore-matrix model for capillary permeability. *Microvasc. Res.* **44,** 85–111.